PAPER

Check for updates

First-principles study of the effect of oxygen vacancy and iridium doping on formaldehyde adsorption on the La₂O₃(001) surface

Youhui Xu,[a] Xiaoying Cao,[a] Xiuwu Chen,[a] Fanting Kong,[a] Hongbo Liang,[a] Hengjiao Gao, [ID] *[b] Hongxia Cao[a] and Jieyu Li[a]

Formaldehyde adsorption on intrinsic La₂O₃ surface, four-fold coordinated oxygen vacancy (VO_{4c}), six-fold coordinated oxygen vacancy (VO_{6c}), and iridium-doped La₂O₃(001) surface was studied by the first-principles method. The results show that formaldehyde adsorption on the Ir-doped La₂O₃(001) surface with VO_{6c} is the strongest because of the directional movement of electrons caused by the interaction of the Ir-5d orbitals and internal oxygen vacancy, wherein the adsorption energy is 3.23 eV. This model showed a significant increase in adsorption energy, indicating that Ir doping improves the formaldehyde adsorption capacity of the La₂O₃(001) surface. The energy band analysis shows that iridium doping introduces impurity energy levels into the intrinsic La₂O₃ energy band, which enhances the interaction between the La₂O₃(001) surface and formaldehyde molecules. Density of state analysis indicated that the adsorption of formaldehyde molecules on the La₂O₃(001) surface is mainly due to the interaction between the O-2p, C-2p orbitals of formaldehyde and the Ir-5d orbital of iridium atoms. Furthermore, the existence of VO_{4c} and VO_{6c} defects has no effect on the position and shape of the valence and conduction bands. The effects of oxygen vacancy and iridium doping on the optical properties mainly appeared in the low-energy infrared and visible regions, making the O-2p, C-2p orbitals of formaldehyde and the Ir-5d, O-2p orbitals of the La₂O₃(001) surface become hybridized near the Fermi level and the electronic transition from the valence band to conduction band more likely to occur. The La₂O₃ material can be used as an ideal photocatalytic material for formaldehyde degradation.

Introduction

Formaldehyde (HCOH) is a colorless, volatile, and pungent-smelling toxic substance that may have a significant impact on human health and the natural environment. Currently, the International Agency for Research on Cancer (IARC) classifies formaldehyde as a group I human carcinogen, and the U.S. Environmental Protection Agency (EPA) lists it as a toxic and harmful water pollutant.[1,2] Long-term exposure to low concentrations of formaldehyde can lead to chronic respiratory diseases, and long-term exposure to high concentrations of formaldehyde may cause severe lung diseases, which are extremely detrimental to human life. Therefore, monitoring and removing indoor formaldehyde is crucial.[3–5] The development of simple, fast, and effective methods to detect and remove formaldehyde completely is attractive and urgent for environmental protection and air purification.[6] Photocatalytic

technology involves the irradiation of a photocatalyst with sunlight at room temperature for increased surface reduction–oxidation ability to achieve pollutant purification, material synthesis, and transformation. Through photocatalytic technology, formaldehyde can be oxidized and decomposed into non-toxic carbon dioxide (CO_2) and water (H_2O).[7,8] The photocatalyst is a critical factor in determining the photocatalytic degradation of formaldehyde. Exploring and developing various potential photocatalysts with high efficiency are important research areas.[9,10] The photocatalysts reported thus far involve s-block elements such as sodium (Na), potassium (K), and strontium (Sr), p-block elements such as gallium (Ga), indium (In), germanium (Ge), and bismuth (Bi), d-block elements such as titanium (Ti), nickel (Ni), cobalt (Co), and zinc (Zn), and La-series elements such as lanthanum (La), cerium (Ce), and samarium (Sm). The photocatalytic degradation of formaldehyde begins from its adsorption and activation on the photocatalyst surface. Therefore, the theoretical study of the adsorption process of formaldehyde can determine the adsorption stability and bonding mechanism between formaldehyde and the substrate surface.[11–13] This can provide a foundation for subsequent studies on the degradation mechanism of formaldehyde. Wu *et al.*[14] studied the mechanism of

[a]School of Media Engineering, Lanzhou University of Arts and Science, Lanzhou 730000, Gansu Province, China

[b]Science and Technology on Vacuum Technology and Physics Laboratory, Lanzhou Institute of Physics, Lanzhou 730000, Gansu Province, China. E-mail: gaohengjiao@163.com

formaldehyde oxidation by manganese (Mn)-doped cerium oxide (CeO_2). They reported that the oxidation included formaldehyde adsorption, C–H bond breaking, formation and desorption of H_2O and CO_2 molecules, a decrease in coordinated oxygen atoms on the surface of the catalyst, and more oxygen vacancies. This lowered the potential barrier of C–H bond breaking and was more conducive to the oxidation of formaldehyde. Alvarado et al.[15] studied the adsorption process of formaldehyde on the surface of monolayer hydrogenated gallium nitride (GaN). They reported that the adsorption of formaldehyde molecules on the N atom and Ga atom sides of the monolayer were physical and exothermic chemical adsorption processes, respectively. The hydrogen atoms adjacent to the surface were captured, and stable methoxy (CH_3O) was formed, resulting in the appearance of a hydrogen vacancy on the surface. Zhang et al.[16] reported that the adsorption of formaldehyde molecules was easier on the bridging oxygen (O) atoms and oxygen vacancies of the $TiO_2(110)$ surface at low temperatures. Zhou et al.[17] studied the adsorption of formaldehyde molecules on Al-doped single-walled carbon nanotubes with vacancies. The interaction between the adsorbed formaldehyde molecules and carbon nanotubes was promoted by the Al doping and the vacancies, resulting in increased adsorption energy and significant charge transfer.

Lanthanum oxide (La_2O_3) has the advantages of a wide bandgap, high dielectric constant, good thermal stability, and low price. It is widely used in the fields of optical glass, catalysts, ceramics, and thermoelectric materials. The wide bandgap semiconductor materials enable the design of photocatalysts with better performance by providing them with various opportunities for modification and a larger space for electronic structure regulation. Since the bandwidth of La_2O_3 is about 5.8 eV, only ultraviolet light can photogenerate the electron–hole pairs.[18] Therefore, the practical applications of La_2O_3 as a photocatalyst are limited due to the low utilization of light energy. Thus, the bandwidth of La_2O_3 should be reduced to respond in infrared light and improve its light absorption efficiency. Loading, doping, and compounding are usually used to improve the photocatalytic activity of photocatalysts. Metal ion doping effectively extends the absorption region of wide-bandgap photocatalysts to the visible region.[19,20] It has been reported that the La_2O_3 surface has good adsorption capacity and activation performance.[21] It has wide application prospects as a photocatalyst for the degradation of indoor formaldehyde. Studies on the formaldehyde degradation by La_2O_3 photocatalysts and its mechanism have not been reported. With the explosive growth in computer performance, computing power and the continuous development of quantum mechanics theory,[22–26] a first-principles calculation based on density functional theory (DFT) was used to study the modification of La_2O_3 due to formaldehyde adsorption and oxidation processes. Li et al.[27] theoretically studied the oxidative changes in $La_2O_3(001)$ and (011) surfaces after La atoms were substituted by different doped cations, such as Cu, Zn, Mg, Fe and Al. They reported that the doping of cations reduced the vacancy-formation energy of La_2O_3 surfaces, effectively improving its catalytic performance. Cong et al.[28] studied the activity change on Sr-doped La_2O_3 due

to the catalytic oxidative coupling of methane. The result indicated that Sr-doped La_2O_3 clusters had higher thermodynamic and kinetic activity due to the catalytic oxidative coupling of methane, wherein the formed Sr–O bond had stronger reactivity with methane and a lower energy barrier to overcome the reaction with methane than the La–O bond. Bannikov et al.[29] reported that the bonding of the doped elements had a significant impact on the magnetic properties of La_2O_3. The nitrogen (N)-doped La_2O_3 combined with six ligands had magnetic, narrow-band semiconductor characteristics. In contrast, the N-doped La_2O_3 combined with four ligands had magnetic, semi-metallic characteristics. At present, there are no relevant reports on the adsorption of formaldehyde molecules on different structures of the La_2O_3 surface. Relevant studies can provide a theoretical basis for the application of La_2O_3 as an efficient photocatalyst in the removal of indoor formaldehyde by photocatalysis technology.

It has been widely reported that La_2O_3 has increased activity in chemical reactions. The adsorption behavior of formaldehyde molecules on the La_2O_3 surface will help to understand the fundamental principles of its increased activity. Herein, the adsorption processes of formaldehyde molecules on the surface of intrinsic La_2O_3, La_2O_3 with oxygen vacancy, and iridium-doped La_2O_3 were studied. The influence of the oxygen vacancy and iridium doping on the adsorption process of formaldehyde molecules was studied. The adsorption energy, density of states, and optical properties of formaldehyde molecules on La_2O_3 with different surface states were calculated, and the bonding characteristics and adsorption mechanism of formaldehyde molecules on the La_2O_3 surface were studied.

Modeling and calculating methods

Modeling

La_2O_3 has a hexagonal crystal structure with the space group of $P\bar{3}m1$. As shown in Fig. 1, the bulk phase structure of La_2O_3 is the superposition of two layers of $(LaO)_n^{n+}$ and one layer of O^{2-}. The La atoms are seven coordinated and marked as La_{7c}. The O atoms, which are four- (2/3 share) and six-coordinated (1/3 share), are marked as O_{4c} and O_{6c}, respectively.[30] The cell parameters of La_2O_3 are given as $a = b = 3.939$ Å, $c = 6.136$ Å, $\alpha = \beta = 90°$, and $\gamma = 120°$. The cell parameters of La_2O_3 were optimized to verify the rationality of the pseudopotential atomic calculations in La_2O_3.

The bulk La_2O_3 is an indirect bandgap semiconductor, wherein the valence band top is mainly composed of the 2p orbital of the O atom and the conduction band is mainly composed of the 5d orbital of the La atom. We validate the effectiveness of the DFT method by calculating the error between the theoretical and experimental values of the lattice parameters. If the error is less than 5%, it indicates that the theoretical simulation method is effective. The optimized cell parameters are $a = b = 3.963$ Å, $c = 6.179$ Å, $\alpha = \beta = 90°$, and $\gamma = 120°$. The errors are less than 1% compared with the initial values, indicating that the pseudopotential atomic calculations and the selection of calculation parameters were reasonable.
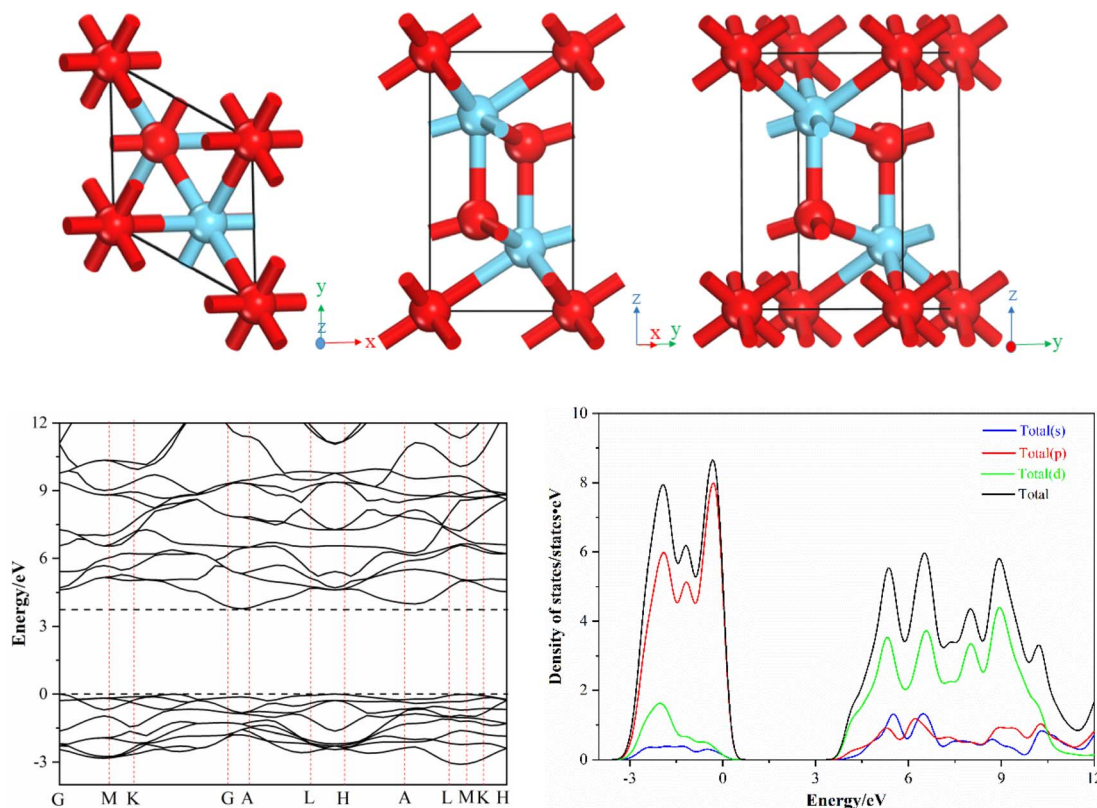
Fig. 1 Bulk phase structure, band structure and DOS of bulk La$_2$O$_3$.

In this paper, the most common and stable La$_2$O$_3$(001) surface was selected as the studied object.[31–33] The inclusion of more atomic layers in the calculation leads to higher accuracy. However, including too many atomic layers in the analysis will increase its cost and reduce its efficiency. In general, a model will represent the properties of the bulk material when the number of atomic layers exceeds 5. In this study, the number of atomic layers was set as 6, and the procedure of the supercell model of the La$_2$O$_3$(001) surface is as follows. First, the cell model of La$_2$O$_3$ was imported from the software model library. Second, we cut the surface in the (001) direction through the surfaces-cleave surface instruction of the Build menu. Third, according to the symmetry-Supercell instruction in the Build menu bar, we inputted 2 and 2 at the U and V positions, respectively, and an expanded cell structure of the section plane was formed. Four, in order to eliminate the impact of the interaction between periodic units, the Crystals-Build Vacuum Slab Crystal instruction in the Build menu was selected and the value of 15 Å was input in the vacuum layer thickness field. Then, the build button was clicked, and a $p(2 \times 2 \times 2)$ supercell model of La$_2$O$_3$(001) is finally obtained. The total number of atoms in the surface model is forty, of which sixteen are La atoms, sixteen are four-coordinated oxygen atoms, and eight are six-coordinated oxygen atoms. After replacing one iridium atom or removing one oxygen atom, the corresponding concentrations are 6.25%, 6.25%, and 12.50%, respectively. In order to make the established La$_2$O$_3$ surface model consistent with the actual situation, the bottom three atomic layers of the La$_2$O$_3$

surface model are constrained. They remain stationary during the model optimization and performance simulation process, and are regarded as La$_2$O$_3$ bulk materials. The three upper layers are not constrained and fully relaxed to simulate the active atoms of the La$_2$O$_3$ surface. There are two types of O atoms in the La$_2$O$_3$ surface model, corresponding to the two modes of oxygen vacancies: four-fold coordinated oxygen vacancy (VO$_{4c}$) and six-fold coordinated oxygen vacancy (VO$_{6c}$). Consequently, as shown in Fig. 2, there are two models of Ir-doped La$_2$O$_3$(001) denoted as IrLa–VO$_{4c}$ and IrLa–VO$_{6c}$, respectively.

In the adsorption modeling process of the formaldehyde molecule on the La$_2$O$_3$(001) surface of the $(2 \times 2 \times 2)$ supercell, the C and O atoms of the formaldehyde molecule bond with the O and La atoms on the La$_2$O$_3$(001) surface, respectively. The O atom can bond with the La atom in three possible ways: adjacent adsorption bonding, diagonal adsorption bonding, and single bond adsorption. In this study, the effects of Ir doping and oxygen vacancies on the adsorption of formaldehyde molecules were compared. There are six possible configurations for formaldehyde molecule adsorption, which are as follows: La$_2$O$_3$(001) surface, La$_2$O$_3$(001) surface containing VO$_{4c}$, La$_2$O$_3$(001) surface containing VO$_{6c}$, Ir-doped La$_2$O$_3$(001) surface, Ir-doped La$_2$O$_3$(001) surface containing VO$_{4c}$, Ir-doped La$_2$O$_3$(001) surface containing VO$_{6c}$, Ir-doped La$_2$O$_3$ containing VO$_{4c}$ and VO$_{6c}$ in turn. Additionally, the O atom of the formaldehyde molecule can bond with either the La or Ir atom on the Ir-doped La$_2$O$_3$(001) surface, resulting in 33 adsorption
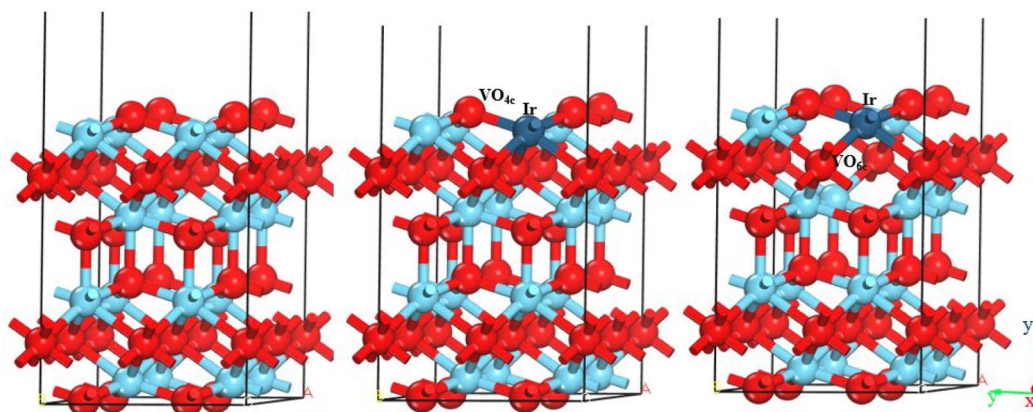
Fig. 2 $p(2 \times 2)$ Ir-doped model of La$_2$O$_3$(001) with different oxygen vacancies.

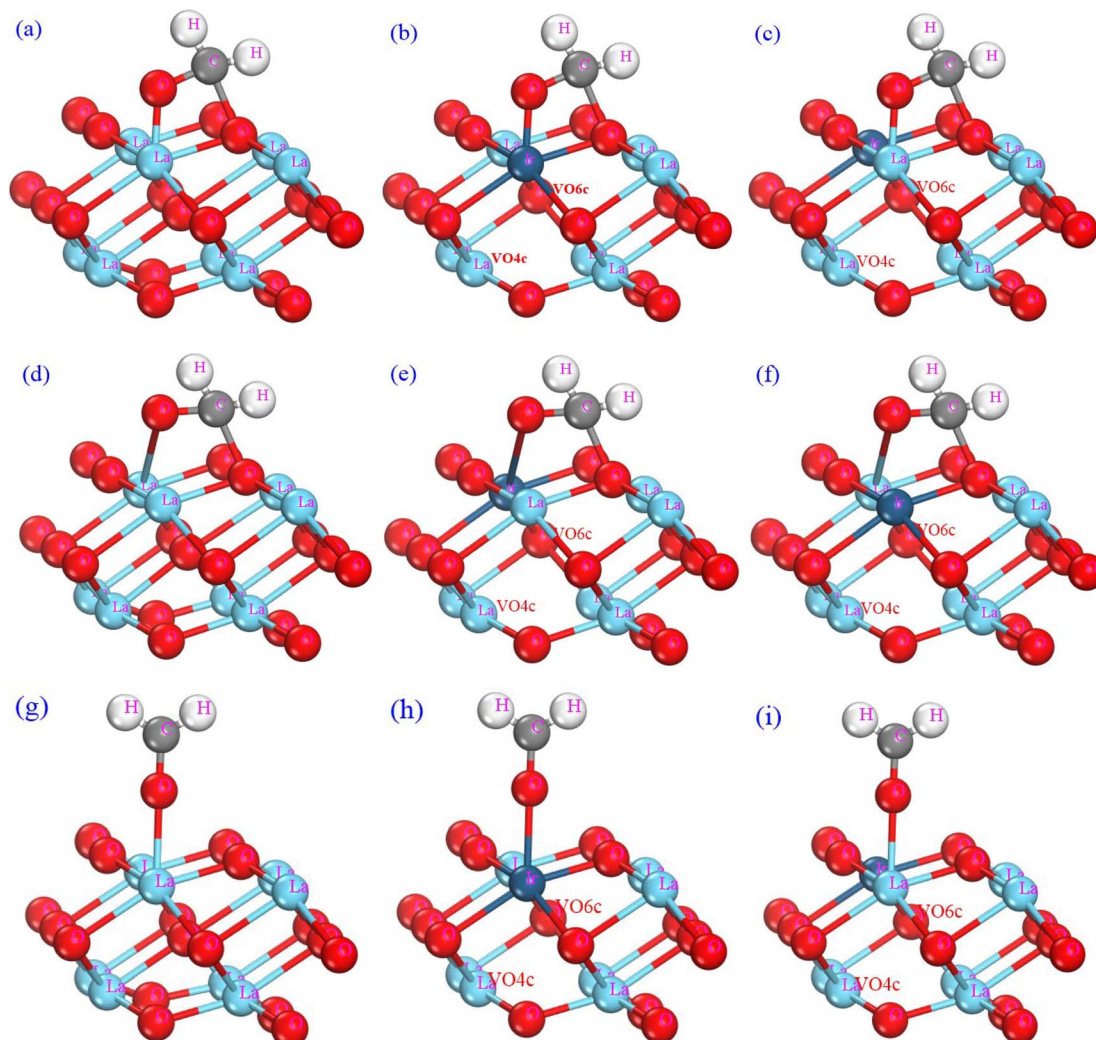**Fig. 3** The adsorption configurations of the formaldehyde molecule on the La$_2$O$_3$(001) surface: (a) adjacent adsorption; (b) adjacent adsorption bonding with the Ir atom; (c) adjacent adsorption bonding with the La atom; (d) diagonal adsorption; (e) diagonal adsorption bonding with the Ir atom; (f) diagonal adsorption bonding with the La atom; (g) single bond adsorption; (h) single bond adsorption bonding with the Ir atom; (i) single bond adsorption bonding with the La atom.

configurations. The formaldehyde molecular adsorption configurations are shown in Fig. 3. The distances of La–O, C–O and C–H are set as 3.0 Å, 3.0 Å and 1.14 Å, respectively. The adsorption energy for each adsorption configuration is different, which impacts the adsorption process significantly.

Calculating methods

The calculations were performed by the CASTEP module of Materials Studio 2019 software based on density functional theory (DFT). The interaction between ions and valence electrons was described by the projected additive wave (PAW) method, and the exchange–correlation potential between electrons was processed by the Perdew–Burke–Ernzerhof (PBE) functional of generalized gradient approximation (GGA).[29,32,33] Through testing, the plane wave truncation kinetic energy was set as 600 eV, the force was distributed to each atom, and the convergence value of the total system energy was less than 3.0×10^{-3} eV nm^{-1} and 1.0×10^{-5} eV per atom, respectively. The deviations of stress and displacement were less than 0.05 GPa and 1.0×10^{-4} nm, respectively. The size of the k lattice point in the Brillouin zone on the La$_2$O$_3$(001) surface was set as $4 \times 4 \times 1$.[34] The valence electron configurations of the La, O, Ir, and C atoms are taken as La 5d^1 6s^2, O 2s^2 2p^4, Ir 4f^{14} 5d^7 6s^2, and C 2s^2 2p^2, respectively.

Results and discussions

Analysis of the adsorption energy calculation results

Adsorption energy (E_{ads}) is defined as the change in total energy of the system before and after adsorption, indicating the stability of the substance in the adsorption system. The sign and calculated value of E_{ads} indicate the possibility and tightness of adsorption, respectively. The equation for E_{ads} is given as follows:[35]

$$E_{ads(AB)} = E_{(CH_2O/La_2O_3(001))} - E_{CH_2O} - E_{La_2O_3(001)} \quad (1)$$

where the $E_{(CH_2O/La_2O_3(001))}$, E_{CH_2O}, and $E_{La_2O_3(001)}$ terms represent the total energy of the system after the formaldehyde is adsorbed on the La$_2$O$_3$(001) surface, the energy of the free formaldehyde molecule, and the energy of the La$_2$O$_3$(001) surface before adsorption, respectively. The adsorption energy refers to that generated during the adsorption process. As the movement speed of the molecules changes from fast to slow in the

adsorption process and finally stops on the substrate surface, a part of the energy will be released due to the reduction of the speed, which is the adsorption energy. It can be considered that the larger the adsorption energy, the greater the bond cooperation between the small molecule and substrate. The E_{ads} indicates the strength of the adsorption effect of the formaldehyde molecule on the La$_2$O$_3$(001) surface. The negative value of E_{ads} indicates that the adsorption process is an exothermic and stable reaction, which can proceed spontaneously. The positive E_{ads} indicates that the adsorption process is an endothermic and unstable reaction that needs an external energy transfer. Generally, the E_{ads} for physical and chemical adsorption processes are -0.62 eV $< E_{ads} < 0$ eV and $E_{ads} < -0.62$ eV, respectively.[36] The calculated E_{ads} values for the adsorption of formaldehyde molecules on different La$_2$O$_3$(001) surface structures are shown in Table 1.

It can be seen that the E_{ads} of adjacent adsorption is the largest, followed by the E_{ads} of diagonal adsorption. The E_{ads} of single bond adsorption is the smallest. Except for the configuration of diagonal adsorption bonding with the Ir atom of the La$_2$O$_3$(001) surface with the VO$_{6c}$ vacancy, the E_{ads} values of all configurations of formaldehyde molecule adsorption on the La$_2$O$_3$(001) surface are negative, indicating that formaldehyde molecules can be spontaneously adsorbed on different La$_2$O$_3$(001) surfaces. The E_{ads} of single bond adsorption bonding with the Ir atom of the Ir-doped and Ir-doped La$_2$O$_3$(001) surfaces with VO$_{4c}$ vacancy is -0.52 eV and -0.32 eV, respectively, indicating a physical adsorption process. The E_{ads} of other adsorption configurations is less than -0.62 eV, indicating a stable chemical adsorption process. The E_{ads} of formaldehyde gas molecules on the La$_2$O$_3$(001) surface is affected by the type of oxygen vacancy, noble metal doping, and the bonding mode of O atoms in formaldehyde molecules. Because of the existence of VO$_{4c}$ in the La$_2$O$_3$ bulk material, the E_{ads} of different adsorption configurations of formaldehyde molecules on the La$_2$O$_3$(001) surface increases. For an intrinsic La$_2$O$_3$(001) surface with VO$_{6c}$ oxygen vacancy, the E_{ads} of the adjacent adsorption configuration decreases, whereas it increases for the diagonal adsorption and single bond adsorption configurations. The E_{ads} for formaldehyde molecules on different La$_2$O$_3$(001) surfaces decreased after the bulk La$_2$O$_3$ is doped with the Ir element, indicating that the Ir doping in La$_2$O$_3$ has an adverse effect on the formaldehyde molecule adsorption. When the VO$_{4c}$ or VO$_{6c}$ oxygen vacancy existed in

Table 1 The calculated E_{ads} values for the adsorption of formaldehyde molecules on different structures of the La$_2$O$_3$(001) surface

Adsorption configuration	Adjacent (eV)		Diagonal (eV)		Single bond (eV)	
	With La	With Ir	With La	With Ir	With La	With Ir
Bulk	−3.07		−1.25		−1.01	
VO$_{4c}$	−3.12		−2.12		−1.04	
VO$_{6c}$	−1.98		−2.47		−1.04	
Ir-doped	−0.97	−1.63	−2.52	−1.25	−1.11	−0.52
Ir-doped and VO$_{4c}$	−1.03	−2.57	−1.22	−0.32	−1.13	−0.99
Ir-doped and VO$_{6c}$	−2.54	−3.23	−2.21	0.46	−0.95	−2.02
Ir-doped, VO$_{4c}$ and VO$_{6c}$	−1.16	−1.83	−1.78	−1.01	−0.85	−0.95

the Ir-doped La$_2$O$_3$(001) surface, the E_{ads} for formaldehyde molecules at the adjacent and single bond top sites increased, and the E_{ads} of the diagonal sites decreased, respectively. The largest E_{ads} is the formaldehyde adsorption on the Ir-doped La$_2$O$_3$(001) surface with VO$_{6c}$ vacancy, which is −3.23 eV. The E_{ads} is larger than that for formaldehyde molecules on the La$_2$O$_3$(001) surface containing an oxygen vacancy, indicating that formaldehyde molecule adsorption benefits the most from the existence of a VO$_{6c}$ oxygen vacancy in Ir-doped La$_2$O$_3$ surface structures. The E_{ads} for formaldehyde molecules on the Ir-doped La$_2$O$_3$(001) surface with VO$_{4c}$ and VO$_{6c}$ vacancy is smaller than that on the La$_2$O$_3$(001) surface with VO$_{6c}$ defects.

The mechanism of the photocatalytic technology of La$_2$O$_3$ semiconductor materials involves four stages. This paper mainly focuses on the adsorption mechanism of formaldehyde molecules on the surface of photocatalytic materials in the first stage. The larger the adsorption energy is, the stronger the adsorption of formaldehyde molecules, and the more conducive to improving the efficiency of the photocatalytic oxidation of formaldehyde molecules. The theoretical research of La$_2$O$_3$ mainly focuses on the surface properties of La$_2$O$_3$, the oxidative coupling of methane (OCM), and the adsorption and desorption of the oxygen molecule. At present, studies on the degradation of formaldehyde by La$_2$O$_3$ photocatalysts and its mechanism have not been reported. Compared with other types of catalyst materials, such as BN (2.14 eV),[5] ZnO (0.85 eV),[12] CeO$_2$ (0.86–1.31 eV),[14] TiO$_2$ (1.66 eV),[16] aluminum-doped carbon nanotubes (0.65 eV),[17] and others, the adsorption energy of formaldehyde adsorbed on the surface of modified La$_2$O$_3$(001) is calculated to reach 3.23 eV. The adsorption energy has been greatly improved, and it can be theoretically used as an ideal photocatalytic material for formaldehyde degradation.

Adsorption mechanism of formaldehyde molecules on the La$_2$O$_3$(001) surface

The energy band structure analysis. The energy band structures of the intrinsic and Ir-doped La$_2$O$_3$(001) surfaces with VO$_{6c}$ defect before and after formaldehyde molecule adsorption along the high symmetry direction of the Brillouin region are shown in Fig. 4. The Fermi energy level is selected at zero point of energy in the process of drawing. It can be seen that the base of the conduction band is near the Fermi level. From Fig. 4a, the valence band maximum (VBM) and conduction band minimum (CBM) are located at the highly symmetric K and M points, respectively. Therefore, the intrinsic La$_2$O$_3$(001) surface is an indirect band gap semiconductor material. After doping the Ir element in the La$_2$O$_3$(001) surface with VO$_{6c}$ oxygen vacancy, the band gap is obviously reduced and more energy levels are increased in the valence band and conduction band (shown in
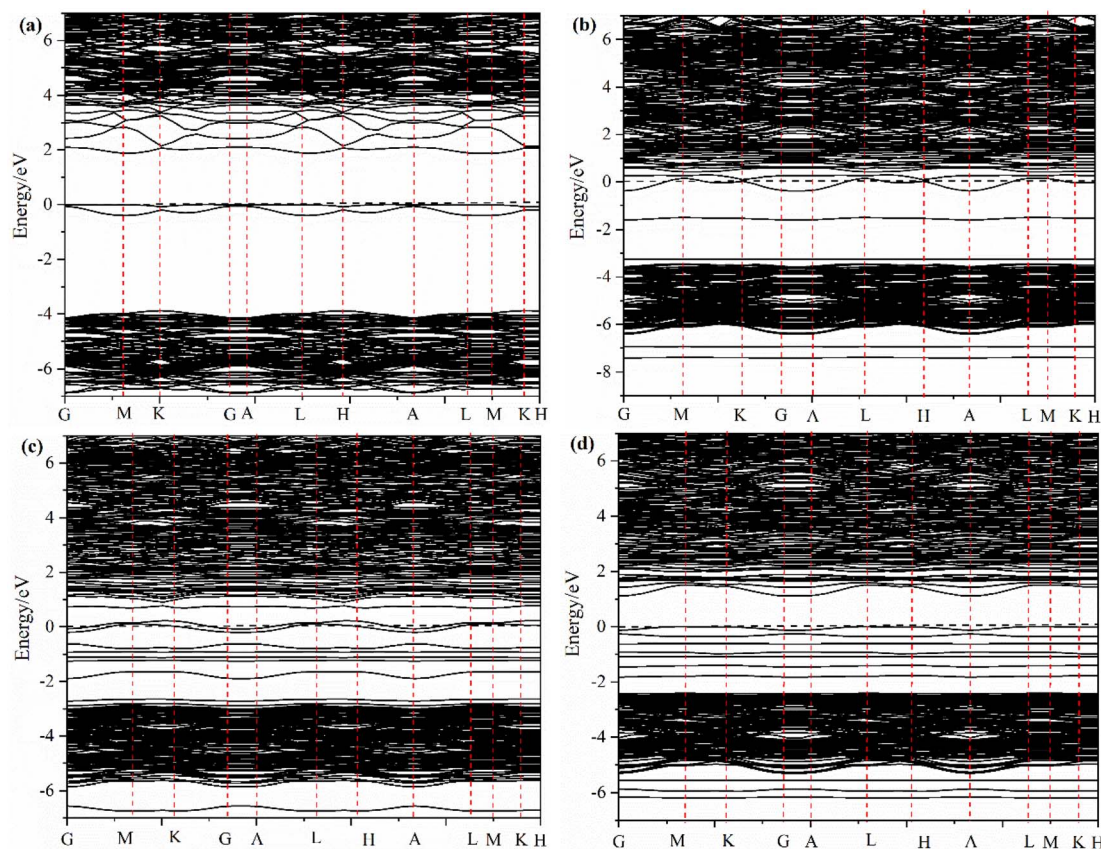

Fig. 4 The band structure of different La$_2$O$_3$(001) surface structures and adsorbed formaldehyde molecule: (a) intrinsic La$_2$O$_3$(001) surface; (b) Ir-doped La$_2$O$_3$(001) surface with VO$_{6c}$ oxygen vacancy; (c) formaldehyde molecule adsorbed on the intrinsic La$_2$O$_3$(001) surface; (d) formaldehyde molecule adsorbed on the Ir-doped La$_2$O$_3$(001) surface with the VO$_{6c}$ oxygen vacancy.

Fig. 4b). Due to the 5d orbital effect of the Ir atom, the impurity level appears in the band gap. In addition, an energy level line appears not far above the top of the valence band. The energy band structure after the adsorption of the formaldehyde molecule in the intrinsic $La_2O_3(001)$ surface is shown in Fig. 4c. It can be seen that the band gap is reduced, and the VB and CB move towards the direction of low energy as a whole. Because of the bonds between the La atom with the O atom, and the O_{4c} atom with the C atom of the formaldehyde molecule, there are many impurity levels appearing above the valence band. The energy band structure of the Ir-doped $La_2O_3(001)$ surface with the VO_{6c} oxygen vacancy after adsorption of the formaldehyde molecule is shown in Fig. 4d. Compared with the formaldehyde molecule adsorbed on the intrinsic $La_2O_3(001)$ surface, a impurity level appears above the valence band due to the action of the Ir-5d orbital.

The effect of the oxygen vacancy and iridium doping on the energy band structure before and after adsorption of formaldehyde molecules on the $La_2O_3(001)$ surface can be summarized as follows. Compared with the intrinsic $La_2O_3(001)$ surface, the new energy levels between the top of the valence band and the bottom of the conduction band enhances the electronic transition process because of the interaction of the 2p orbital of the oxygen vacancy atoms and the 5d orbital of the Ir atom, which acts as a bridge and is conducive to the electronic transition process.

The density of states analysis. The density of states of the intrinsic and the Ir-doped $La_2O_3(001)$ surface structures and VO_{6c} oxygen vacancy are shown in Fig. 5, where the Fermi energy level is taken at zero energy. In Fig. 5a, the intrinsic $La_2O_3(001)$ surface structure shows two peaks for the valence band (VB) in the high energy range (-6.89 eV to -3.02 eV) and different contributions of O atoms with different coordination numbers. The peak in the high energy direction is mainly due to the action of electrons on the VO_{6c}-2p and La-5d orbitals. In contrast, the peak in the low-energy direction is mainly due to the action of electrons on the VO_{4c}-2p and La-5d orbitals. The peak in the low energy range (-21.68 eV to -15.19 eV) is due to the action of electrons on the O-2s and La-5p orbitals. The energy range corresponding to the conduction band (CB) (-1.13 eV to 21.30 eV) is mainly due to the action of electrons on the La-5d and O-2p orbitals and the action of a few electrons on the La-6s and La-5p orbitals. The electronic energy state on top of the valence band is mainly contributed by the O_{6c}-2p orbital in the lamella. In contrast, the lower electronic energy state is contributed by the O_{4c}-2p orbital of the surface. Therefore, it is considered that the activity of the $La_2O_3(001)$ surface structure is determined by the O_{6c} oxygen vacancy.

In Fig. 5b, the shapes of the peak and corresponding energy intervals in the high-energy conduction band and low-energy valence band agree with the density of states analysis. The Ir-doped and VO_{6c} oxygen vacancy do not have a significant effect on the valence band. However, the density of state peak of the O_{4c}-2p orbital splits and broadens due to Ir doping, Ir atom bonding with O_{4c}, electron transfer from the Ir atom to O_{4c}, and interaction between the Ir-5d orbital and O_{4c}-2p orbital. Furthermore, Ir doping and O_{6c} enable the La-5p orbital to play
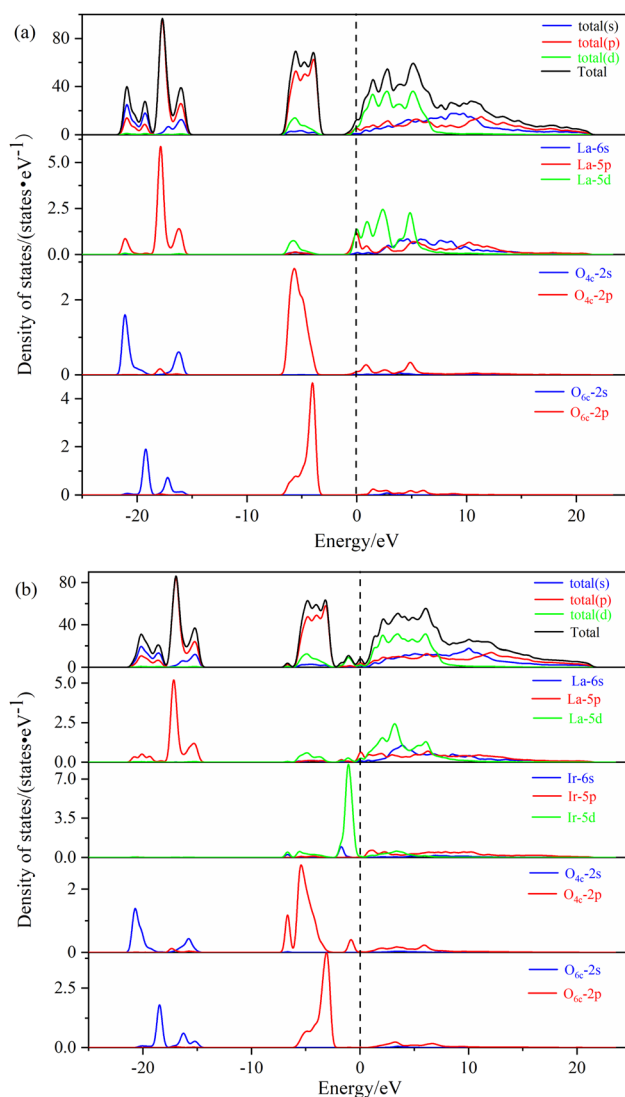

Fig. 5 The density of states of different $La_2O_3(001)$ surface structures: (a) intrinsic $La_2O_3(001)$ surface; (b) Ir-doped $La_2O_3(001)$ surface with VO_{6c} oxygen vacancy.

an important role near the Fermi level. Therefore, two new peaks of the density of states emerge close to the conduction and valence bands, which is conducive to the electronic transition process.

The density of states of free formaldehyde molecules, intrinsic $La_2O_3(001)$ surface, and Ir-doped $La_2O_3(001)$ surface with VO_{6c} oxygen vacancy are shown in Fig. 6. As shown in Fig. 6a, the peaks of the merged and orbital electron density of states for free formaldehyde molecules are sharp and narrow with high localization, which is consistent with the density of states characteristics for general gaseous molecules. After the formaldehyde molecules are adsorbed on the $La_2O_3(001)$ surface, the orbitals broaden and merge, and the orbital electrons show typical delocalization, which is due to interaction between the formaldehyde molecules and surface atoms. As shown in Fig. 6b, the density of states of the intrinsic $La_2O_3(001)$ surface changes significantly after adsorption of formaldehyde
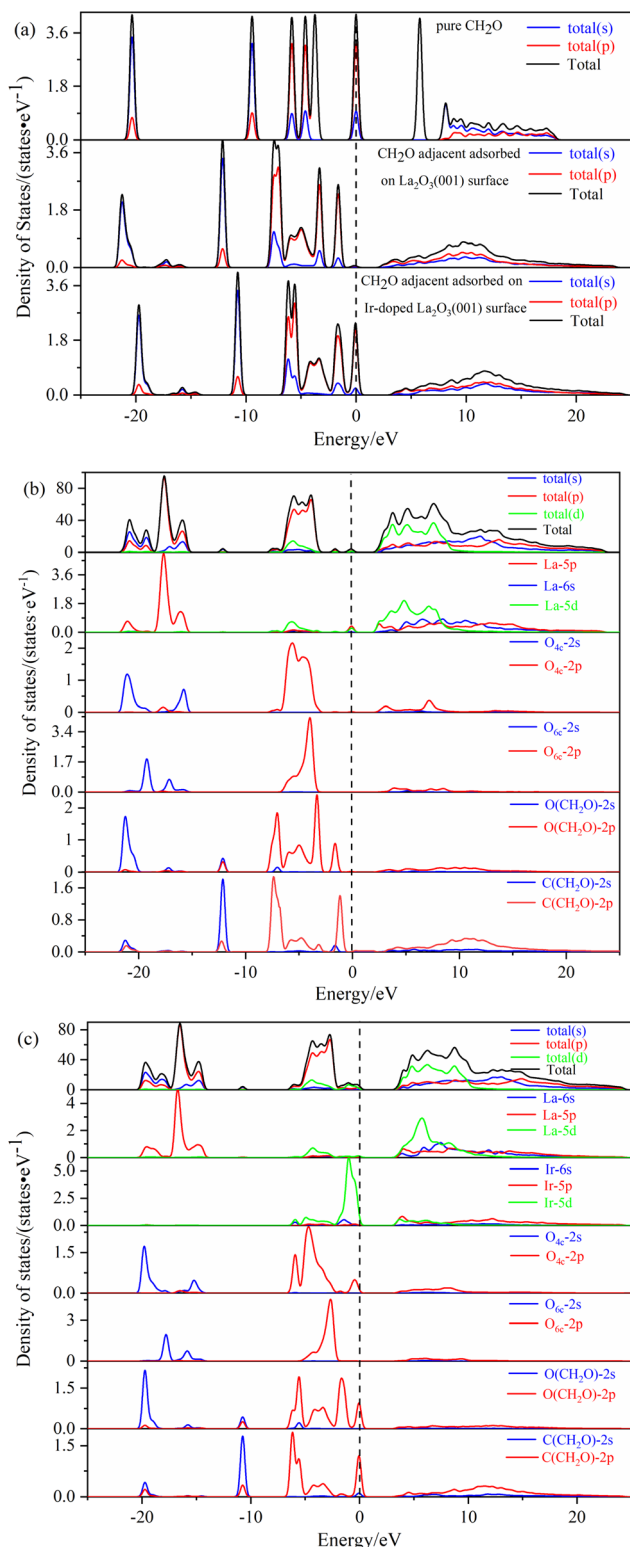
Fig. 6 The density of states for: (a) free formaldehyde; (b) formaldehyde adjacent adsorbed on the $La_2O_3(001)$ surface; (c) formaldehyde adjacent adsorbed on the Ir-doped $La_2O_3(001)$ surface with VO_{6c} oxygen vacancy.

molecules. The conduction band shifts to a high-energy direction, and two new isolated peaks of the density of states appear between the valence and conduction bands of the intrinsic $La_2O_3(001)$ surface structure. The peak at the Fermi level is due to the La-5p orbital. The peak in the low-energy direction is due to hybridization of the O-2p and C-2p orbitals in formaldehyde molecules. This indicates that there is a strong interaction between a single formaldehyde molecule and the $La_2O_3(001)$ surface. Upon adsorption of formaldehyde molecules, impurity levels are generated between the conduction and valence bands. These impurity levels hinder the charge transfer after subsequent adsorption of formaldehyde molecules, which results in the unstable adsorption of more formaldehyde molecules. Fig. 6c shows that the two isolated peaks for the density of states between the conduction band and the valence band disappear. For the Ir-doped $La_2O_3(001)$ surface structure containing VO_{6c} defects, the peak for the density of states of the valence band widens and extends to a position near the Fermi level. The top of the valence band is due to the Ir-5d and O_{4c}-2p orbitals and the O-2p and C-2p orbitals of the formaldehyde molecules. The doping of Ir atoms in the $La_2O_3(001)$ surface structure causes the hybridization of the O-2p and C-2p orbitals of formaldehyde molecules and the Ir-5d and O_{4c}-2p orbitals of the surface layer, resulting in an easier transfer of the lone pair of electrons in the formaldehyde molecules to the $La_2O_3(001)$ surface. Therefore, the VO_{6c} defect and Ir doping reduce the gap between the valence and conduction bands and enhance the interaction between the formaldehyde molecules and $La_2O_3(001)$ surface by promoting charge transfer. Consequently, the same $La_2O_3(001)$ surface area adsorbs more formaldehyde molecules.

Electronic structures of different $La_2O_3(001)$ surfaces before and after formaldehyde molecule adsorption. The density of states of seven different $La_2O_3(001)$ surface structures before and after formaldehyde molecules adsorption are shown in Fig. 7. It can be seen that the existence of VO_{4c} or VO_{6c} oxygen vacancy has no effect on the position and shape of the valence and conduction bands. The bottom of the conduction band is located near the Fermi level. The bandgap of the intrinsic $La_2O_3(001)$ surface is similar to that of the $La_2O_3(001)$ surface with the VO_{4c} oxygen vacancy, while the bandgap of the $La_2O_3(001)$ surface with the VO_{6c} defect is significantly increased. The charge transfer during the adsorption of the formaldehyde molecules is hindered, and interaction between formaldehyde molecules and the $La_2O_3(001)$ surface is weakened. Consequently, the E_{ads} of the formaldehyde molecules on the $La_2O_3(001)$ surface containing the VO_{6c} oxygen vacancy is dramatically smaller than that of the other two surface structures. The peak distribution of the density of states changes after Ir doping of the $La_2O_3(001)$ surface. The peak shifts towards the high-energy direction, and the top of the valence band is located near the Fermi level. The Ir doping of the $La_2O_3(001)$ surface enables the Ir-5d orbital to contribute to the formation of the top of the valence band of the $La_2O_3(001)$ surface. The complete valence band extends a peak on the density of states figure, thus providing more electronic orbitals at the top of the valence band. However, compared with the bandgaps of the Ir-doped $La_2O_3(001)$ surface, the Ir-doped $La_2O_3(001)$ surface with the VO_{4c} oxygen vacancy, and the Ir-doped $La_2O_3(001)$ surface with the VO_{4c} and VO_{6c} oxygen vacancies, it had no noticeable change before and after
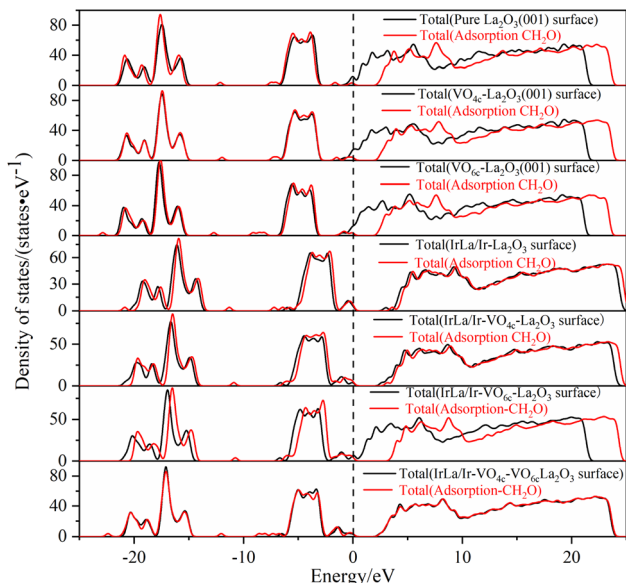
Fig. 7 The density of states of different La_2O_3(001) surface structures before and after the adsorption of a formaldehyde molecule.

formaldehyde molecule adsorption. The bandgaps increased compared with the surfaces of the adjacent adsorption, diagonal adsorption and single bond adsorption configuration, which are opposite to the electronic transition. The increase of the La and Ir atomic charges in the upper two layers is a result of the downward movement of electrons, which is located in the third atomic layer and far from the surface layer, making the uneven charge distribution in the three upper atomic layers more significant. These adsorption configurations will result in materials with almost zero bandgaps, and lead to the electronic transition proceeding more easily. Therefore, because of the directional movement of electrons caused by the significant Ir-5d orbital and internal oxygen vacancies, the formaldehyde molecule adsorption on the Ir-doped La_2O_3(001) surface with VO_{6c} oxygen vacancy is most likely an adsorption configuration.

Therefore, based on the above research results, we summarize the conclusion as follows. The physical nature of oxygen vacancy and iridium doping on the electronic properties before and after the adsorption of formaldehyde molecules on the La_2O_3(001) surface is the interaction of the 2p orbital of the oxygen vacancy atoms and 5d orbital of the Ir atom, which forms new energy levels between the top of the valence band and the bottom of the conduction band. These energy levels provide a bridge that facilitates the excited transition of valence band electrons towards the conduction band. After the adsorption of formaldehyde molecules on the La_2O_3(001) surface, the transition electrons will react with the C-2p and O-2p orbital electrons of the formaldehyde molecules. Subsequently, the oxidative degradation of formaldehyde molecules occurs. Compared with the intrinsic La_2O_3(001) surface, the Ir-doped La_2O_3(001) surface with oxygen vacancy significantly enhanced the adsorption of formaldehyde and interaction between the orbital electrons, which is more conducive to the process of formaldehyde oxidative degradation.

Optical properties

The dielectric function $\varepsilon(\omega)$. Semiconductor materials can be regarded as continuous media in the ultraviolet to visible wavelength range. The corresponding macro-optical function can be described using a complex dielectric function. As expressed by eqn (2),[37,38] the dielectric function $\varepsilon(\omega)$, which reflects the relationship of the energy band, is a bridge between the microphysical process of the interband transition and the solid electronic structure:

$$\varepsilon(\omega) = \varepsilon_1(\omega) + i\varepsilon_2(\omega) \tag{2}$$

where ω represents the frequency of the incident light, and $\varepsilon_1(\omega)$ and $\varepsilon_2(\omega)$ represent the real and imaginary parts of the dielectric function, respectively. The reflection spectrum and absorption spectrum are determined by $\varepsilon_1(\omega)$ and $\varepsilon_2(\omega)$ of the dielectric function, respectively.

The first-principles method was used to calculate the optical properties of different La_2O_3(001) surface structures and the formaldehyde molecules after adsorption. Furthermore, since the calculated value of the bandgap was smaller than the experimental value, the scissor operator was used for the correction. A correction factor of 2.29 eV was used to convert the calculated value of 2.51 eV to the experimental value of 5.8 eV. The curves of the calculated values of the real and imaginary parts of the dielectric function in the selected energy range of 0–10 eV are shown in Fig. 8 and 9. Considering only the electronic contribution to the dielectric constant, it can be seen from Fig. 8 that the static dielectric constants of different La_2O_3(001) surfaces before formaldehyde molecule adsorption are 3.45, 17.14, 6.10, 3.46, 3.16, 2.99 and 3.86, and the corresponding values after formaldehyde molecule adsorption are 3.09, 3.17, 4.74, 3.14, 3.50, 2.98 and 3.25, respectively. Except for the configuration of the diagonal adsorption bonding with the Ir atom of the La_2O_3(001) surface with the VO_{6c} oxygen vacancy, the static permittivities of different La_2O_3(001) surface configurations decrease after the formaldehyde molecules are

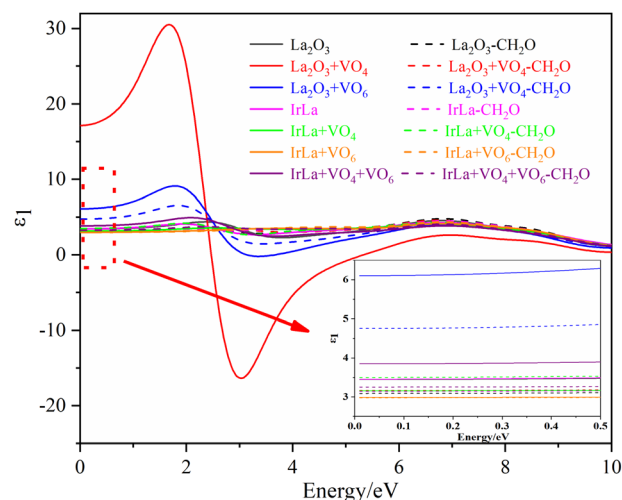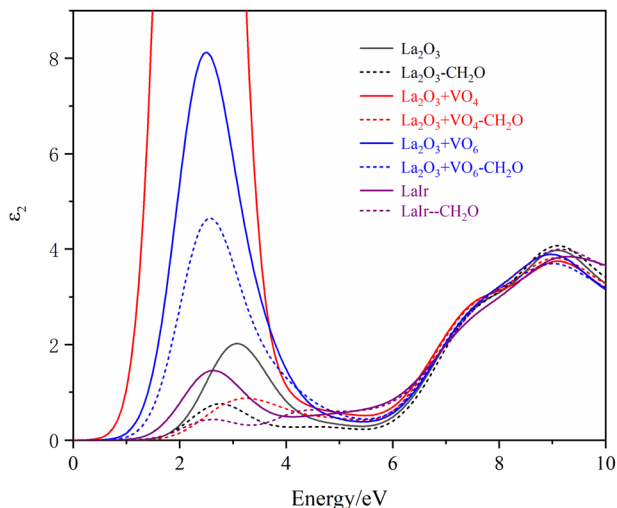**Fig. 8** The real part of the permittivity of different La_2O_3(001) surfaces and adsorbing formaldehyde molecule.

Fig. 9 The imaginary part of the permittivity of different La_2O_3(001) surfaces and the adsorbing formaldehyde molecule.

Fig. 10 The absorption spectra of different La_2O_3(001) surfaces and adsorbed formaldehyde molecule.

adsorbed. In the low energy region (<2 eV), the real part $\varepsilon_1(\omega)$ of the dielectric function increases with an increase in energy and peaks at about 2 eV. The density of states indicates that this is mainly caused by the electronic transition from the La-5d or doped Ir-5d orbital to the O-2p orbital on the La_2O_3(001) surface. As shown in Fig. 9, the peaks of $\varepsilon_2(\omega)$ emerge in two stages with the increase in photon energy. The peak of stage 1 (about 4.74 eV < e < 15.00 eV) is due to an electronic transition from the top of the valence band to the bottom of the conduction band. In addition, the peak of stage 2 (15 eV < e < 40 eV) is due to an electronic transition from the center and top of the valence band to the bottom and center of the conduction band.

The absorption spectrum $\alpha(\omega)$. The absorption spectrum $\alpha(\omega)$ can be calculated according to $\varepsilon_1(\omega)$ and $\varepsilon_2(\omega)$. The formula for $\alpha(\omega)$ is shown as follows.[39]

$$\alpha(\omega) = 2(\omega)[\varepsilon_1^2(\omega) + \varepsilon_2^2(\omega) - \varepsilon_1(\omega)]^{1/2} \quad (3)$$

The calculated absorption spectrum of different La_2O_3(001) surfaces and adsorbing formaldehyde molecule is shown in Fig. 10. It can be seen that the oxygen vacancy and Ir doping have a significant impact on the absorption spectrum of La_2O_3(001) surfaces. Both VO_{4c} and VO_{6c} oxygen vacancies can increase the absorption peak of the La_2O_3(001) surface in the visible region, and Ir doping obviously weakens the absorption intensity in this region. The absorption peaks in the low-power infrared and visible light region disappear when there is a single type of oxygen vacancy or Ir doping on the La_2O_3(001) surface. However, they reappear when the VO_{4c} oxygen vacancy, CO_{6c} oxygen vacancy, and Ir doping exist at the same time. The absorption peaks of adjacent adsorption configurations of different La_2O_3(001) surfaces are located at 3.34 eV (371 nm), 3.03 eV (409 nm), 3.07 eV (404 nm), 2.84 eV (437 nm), and 3.15 (394 nm), and the corresponding absorption edges are 1.68 eV, 0.77 eV, 1.11 eV, 1.32 eV, and 1.30 eV, respectively. This indicates that the La_2O_3(001) surface with the VO_{4c} oxygen vacancy
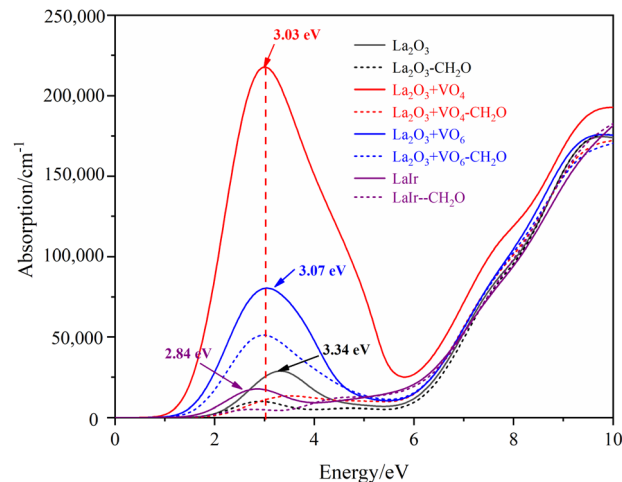
has a stronger long-wave absorption capacity, and the absorption wavelength can extend to the infrared region (1610 nm). The main reason is that the absorption spectrum is determined by the imaginary part $\varepsilon_2(\omega)$ of the dielectric function. Due to the change in the electron distribution near the Fermi level of different La_2O_3(001) surfaces, the absorption band edge and band gap are different. This eventually leads to various degrees of difficulty, and the process of electronic transition from the top of the valence band to the bottom of the conduction band. After the adsorption of formaldehyde molecules on different La_2O_3(001) surfaces, the absorption peaks of other configurations disappeared in the visible region. This is due to the hybridization near the Fermi level between the O-2p, C-2p orbitals of the formaldehyde molecule and the Ir-5d, O_{4c}-2p orbitals of the top atomic layer on the La_2O_3(001) surfaces. The gap between the valence band and conduction band is significantly reduced to form approximately zero band gap materials, such that electronic transitions from the valence band to the conduction band can occur with almost no energy barriers.

The reflection spectrum $R(\omega)$. The reflection spectrum $R(\omega)$ can be calculated from $\varepsilon_1(\omega)$ and $\varepsilon_2(\omega)$, as shown in the following equation:[40]

$$R(\omega) = \left| \frac{\sqrt{\varepsilon_1(\omega) + i\varepsilon_2(\omega)} - 1}{\sqrt{\varepsilon_1(\omega) + i\varepsilon_2(\omega)} + 1} \right|^2 \quad (4)$$

The $R(\omega)$ is the macroscopic manifestation of a solid electronic interband transition under the perturbation of an optical electromagnetic field, which is determined by the real part of the dielectric function. Fig. 11 shows the calculated absorption spectra of different La_2O_3(001) surfaces and adsorbed formaldehyde molecule. It can be seen that the variation trends of the reflection spectrum and absorption spectrum are similar. Furthermore, the reflectivity increases with increasing photon energy in the low-energy infrared and visible regions. Because of the interaction between reflection and absorption, the La_2O_3(001) surface effectively reflects light in a certain range. It
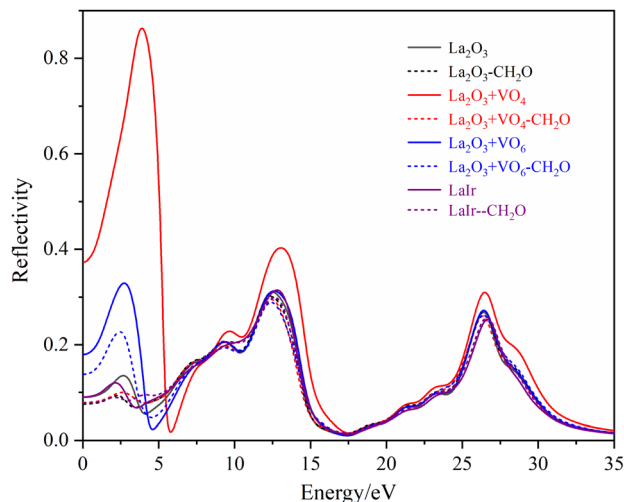
Fig. 11 The reflectance spectra of different La_2O_3(001) surfaces and adsorbed formaldehyde molecule.

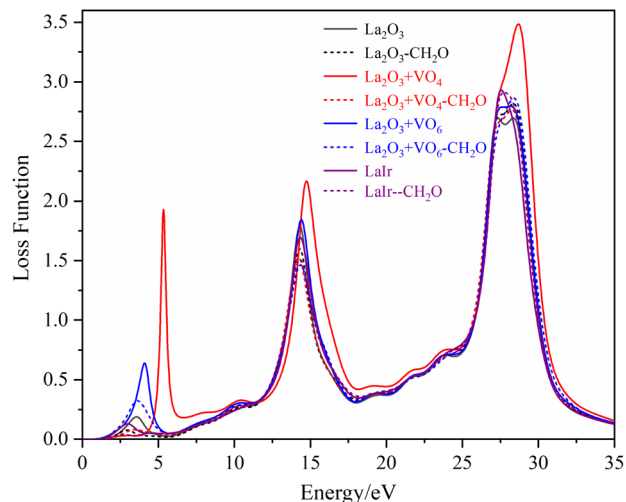**Fig. 12** The loss functions of different La_2O_3(001) surfaces and adsorbed formaldehyde molecule.

can also absorb light in the same wavelength range. There are three reflection peaks on the adjacent adsorption configurations of different La_2O_3(001) surfaces, and the corresponding energies are located at around 2.65 eV, 12.70 eV, and 26.45 eV, respectively, whereas the reflection spectra of the La_2O_3(001) surfaces with the single oxygen vacancy (VO_{4c} or VO_{6c}) and Ir doping only have two peaks at 12.70 eV and 26.45 eV. After adsorption of formaldehyde molecules, the reflection peaks in the low-energy infrared and visible regions near 2.65 eV disappear, and the reflection spectrum contains two peaks near 12.70 eV and 26.45 eV.

The energy loss function $L(\omega)$. The energy loss function represents the absorption state of the photoelectron energy when it passes through the interior of the homogenous dielectric, and the peak value represents the properties associated with the plasma resonance absorption. The energy loss spectrum represents the outer electrons of the solid material absorbing energy and then transitioning to a higher orbital. Thus, the band gap and bond strength can be analyzed according to the information from the spectrum, from which the material type can be determined by the energy loss function. In a homogeneous dielectric, the Coulomb field amplitude and intensity of the incident photoelectron are screened to $1/\varepsilon$ and $1/\varepsilon^2$, respectively. When a photoelectron passes through the dielectric, the motion process is delayed, and the energy attenuation is proportional to the field intensity ε^2, which is the imaginary part of the dielectric function. Therefore, the energy loss function $L(\omega)$ can be calculated by the following formula:[41]

$$L(\omega) \propto \frac{\varepsilon_2(\omega)}{|\varepsilon(\omega)|^2} = \mathrm{Im}\left(\frac{-1}{\varepsilon(\omega)}\right) = \frac{\varepsilon_2(\omega)}{\varepsilon_1{}^2(\omega) - \varepsilon_2{}^2(\omega)} \quad (5)$$

The loss functions of different La_2O_3(001) surfaces and adsorbed formaldehyde molecule are shown in Fig. 12. There are three main peaks in the energy loss function spectrum. The corresponding energy and change trend are basically consistent with the reflection spectrum. Conversely, the change in the peak

value is opposite to the high value of the reflection peak, which corresponds to the low value of the peak in the energy loss function spectrum. The peak position represents the frequency of the excited electron and vibrational frequency of the particles. The peak of the energy loss function corresponds to the sharp drop area of the reflection peak, and all of the peak values are within the energy range of 1–50 eV.

Conclusions

The effects of the oxygen vacancy (VO_{4c} and VO_{6c}) and iridium doping on formaldehyde adsorption on the La_2O_3(001) surface were studied by the first-principles method. From the view of energy, the adjacent adsorption of the iridium-doped La_2O_3(001) surface containing the VO_{6c} oxygen vacancy is the most stable adsorption site for formaldehyde molecules. Due to the significant doping of the Ir-5d orbital and internal VO_{6c} oxygen vacancies, the effects of the oxygen vacancy and iridium doping on the optical properties of the La_2O_3(001) surface are mainly shown in the low-energy infrared and visible regions.

Compared with the ZnO, CeO_2, TiO_2, and Al-doped carbon nanotube catalyst materials, the E_{ads} of formaldehyde adsorbed on the modified La_2O_3(001) surface is 3.23 eV, which is a significant improvement. The La_2O_3 semiconductor material can be used as an ideal photocatalytic material for formaldehyde degradation and indoor detection of formaldehyde gas. In the subsequent research process, we will start the technical study on the noble metal iridium doping of La_2O_3 by atomic layer deposition technology and photocatalytic degradation of formaldehyde, and conduct an overall evaluation of the performance and application prospect of the La_2O_3 photocatalytic material.

Data availability

The data that support the findings of this study can be obtained from the corresponding author. Hengjiao Gao, Email: gaohengjiao@163.com.

Conflicts of interest

There are no conflicts to declare.

Acknowledgements

References

1 S. E. Diltemiz and K. Ecevit, High-performance formaldehyde adsorption on CuO/ZnO composite nanofiber coated QCM sensors, *J. Alloys Compd.*, 2019, **783**, 608–616.

2 A. Noguerón, H. N. Fernández-Escamilla, J. Guerrero-Sánchez and N. Takeuchi, Formaldehyde adsorption on a hydrogenated aluminum nitride monolayer: a self-propagated reaction, *Comput. Theor. Chem.*, 2019, **1159**, 18–22.

3 M. W. Zheng, Y. T. Lin and S. H. Liu, $TiO_2@g-C_3N_4/SiO_2$ with superior visible-light degradation of formaldehyde for indoor humidity control coatings, *Mater. Today Sustain.*, 2023, **24**, 100496.

4 J. Pei, Z. Bai, Y. Pan and Q. Wu, Long-lasting removal of indoor formaldehyde in continuous airflow by $B–TiO_2@AC$ composites, *Built Environ.*, 2024, **256**, 111458.

5 H. Zhang, Z. Zheng, T. Yu, C. Liu, H. Qian and J. Li, Seasonal and diurnal patterns of outdoor formaldehyde and impacts on indoor environments and health, *Environ. Res.*, 2022, **205**, 112550.

6 L. Lu, T. Xiao, X. Yang, X. Zhou and J. Yan, Refinement and predicting formaldehyde concentrations of indoor fabric: effects of temperature and humidity, *Chemosphere*, 2023, **342**, 140096.

7 V. Gupta, S. Sarkar, O. Aftenieva, T. Tsuda, L. Kumar, D. Schletz, J. Schultz, A. Kiriy, A. Fery, N. Vogel, *et al.*, Nanoimprint lithography facilitated plasmonic-photonic coupling for enhanced photoconductivity and photocatalysis, *Adv. Funct. Mater.*, 2021, **31**, 2105054.

8 P. A. F. Cortés, M. Marx, M. Trose and M. Beller, Heteroleptic copper complexes with nitrogen and phosphorus ligands in photocatalysis: overview and perspectives, *Chem Catal.*, 2021, **1**, 298–338.

9 B. Tang, Y. He, Z. Zhang, Z. Wang, L. Ji, T. Ma, S. Li, Y. Dai and G. Zhang, Influence of N doping and the functional groups of graphene on a RGO/TiO_2 composite photocatalyst, *Sci. China: Technol. Sci.*, 2020, **63**, 1045–1054.

10 W. Xie, Q. Fu, C. Cheng, G. Zhang, N. Yan and Z. Wang, Effect of La_2O_3 on the oxidation resistance of SiC ceramic at 1973K: experimental and theoretical study, *J. Am. Ceram. Soc.*, 2020, **103**, 614–621.

11 H. Zhao, K. An, Z. Wang, X. Liu, M. He, X. Yang, Z. Tang, S. Lai, S. Han, Z. Sun and Y. Jiao, The impact of water co-adsorption on the removal of formaldehyde from the indoor air by oxygen-rich activated carbons: a theoretical and experimental study, *Appl. Surf. Sci.*, 2023, **635**, 157729.

12 H. Tran and M. Spencer, Zinc oxide for gas sensing of formaldehyde: density functional theory modeling of the effect of nanostructure morphology and gas concentration on the chemisorption reaction, *Mater. Chem. Phys.*, 2017, **163**, 274–284.

13 J. Xiao, X. Li, H. Lian, M. Pan, C. Xu, C. Xia, S. Lan and W. Li, Deep eutectic solvents for effective removal of indoor formaldehyde: theoretical design, experiment, and adsorption mechanism study, *J. Mol. Liq.*, 2023, **392**, 123473.

14 H. Wu, S. Ma, W. Song and E. J. Hensen, Density functional theory study of the mechanism of formaldehyde oxidation on Mn-doped ceria, *J. Phys. Chem.*, 2016, **120**, 13071–13077.

15 L. A. Alvarado-Leal, H. N. Fernandez-Escamilla, J. Guerrero-Sanchez, E. Martínez-Guerra and N. Takeuchi, Formaldehyde adsorption on a hydrogenated gallium nitride monolayer: a density functional theory study, *Appl. Surf. Sci.*, 2020, **506**, 144944.

16 Z. Zhang, M. Tang, Z.-T. Wang, Z. Ke, Y. Xia, K. T. Park, I. Lyubinetsky, Z. Dohnalek and Q. Ge, Imaging of formaldehyde adsorption and diffusion on $TiO_2(110)$, *Top. Catal.*, 2015, **58**, 103–113.

17 Q. Zhou, C. Wang, Z. Fu, H. Zhang and Y. Tang, Adsorption of formaldehyde molecule on Al-doped vacancy-defected single-walled carbon nanotubes: a theoretical study, *Comput. Mater. Sci.*, 2014, **82**, 337–344.

18 S. Mirza, M. Zulfiqar and S. Azam, Effect of hydrostatic pressure on electronic, elastic, and optical properties of hexagonal lanthanum oxide (La_2O_3): a first principles calculations, *Phys. B*, 2024, **676**, 415686.

19 S. Li, Y. Lin, Y. Wu, Y. Wu, X. Li and W. Tian, Ni doping significantly improves dielectric properties of La_2O_3 films, *J. Alloys Compd.*, 2020, **822**, 153469.

20 D. Salinas, N. Escalona, G. Pecchi and J. L. G. Fierro, Fierro. Lanthanum oxide behavior in La_2O_3-Al_2O_3 and La_2O_3-ZrO_2 catalysts with application in FAME production, *Fuel*, 2019, **253**, 400–408.

21 S. Li, G. Liu, S. Zhang, K. An, Z. Ma, L. Wang and Y. Liu, Cerium-modified Ni-La_2O_3/ZrO_2 for CO_2 methanation, *J. Energy Chem.*, 2020, **43**, 155–164.

22 M. Du, J. Zheng, L. Mei, Y. Zhang and C. Hou, Exploring the conversion mechanism of formaldehyde to CO_2 and H_2 catalyzed by bifunctional ruthenium catalysts: a DFT study, *Mol. Catal.*, 2022, **530**, 112630.

23 C. Parks, K. Hughes and M. Pourkashanian, Furthering the understanding of product formation in monoethanolamine degradation: a mechanistic DFT study, *Int. J. Greenhouse Gas Control*, 2022, **119**, 103732.

24 J. Sun, W. Du, B. Xiao, Y. Wu, Y. Liu and T. Zhang, First-principles study of multiple-site substitutions of alloying elements in Ni-based single crystal superalloys, *Sci. China: Technol. Sci.*, 2021, **64**, 1276–1284.

25 L. Liu and J. Zhao, Formaldehyde adsorption and decomposition on rutile (110): a first-principles study, *Surf. Sci.*, 2016, **652**, 156–162.

26 V. Nagarajan and R. Chandiramouli, DFT investigation of formaldehyde adsorption characteristics on MgO nanotube, *J. Inorg. Organomet. Polym.*, 2014, **24**, 1038–1047.

27 B. Li and H. Metiu, DFT studies of oxygen vacancies on undoped and doped La_2O_3 surfaces, *J. Phys. Chem. C*, 2010, **114**, 12234–12244.

28 L. Cong, Y. Zhao, S. Li and Y. Sun, Sr-doping effects on La_2O_3 catalyst for oxidative coupling of methane, *Chin. J. Catal.*, 2017, **38**, 899–907.

29 V. Bannikov, I. Shein and A. Ivanovskii, Magnetic and electronic properties of nitrogen-doped lanthanum sesquioxide La_2O_3 as predicted from first principles, *J. Supercond. Novel Magn.*, 2011, **24**, 1693–1696.

30 C. Liu, X. Fan and S. Ahmed, Structures and electronic properties of four crystal GeO_2 and two rare-earth element oxides La_2O_3 and CeO_2: first principles calculation, *J. Theor. Comput. Chem.*, 2013, **5**, 1350031.

31 Z. Wang, D. Wang and X. Gong, Strategies to improve the activity while maintaining the selectivity of oxidative coupling of methane at La_2O_3: a density functional theory study, *ACS Catal.*, 2020, **10**, 586–594.

32 W. Cheng, W. Xia and H. Wan, Influence of surface reactivity of lanthanum oxide on the activation of methane and oxygen, *Chem. J. Chin. Univ.*, 2019, **40**, 940–949.

33 M. S. Palmer, M. Neurock and M. M. Olken, Periodic density functional theory study of the dissociative adsorption of molecular oxygen over La_2O_3, *J. Phys. Chem. B*, 2022, **106**, 6543–6547.

34 S. Wang, S. Li and D. A. Dixon, Mechanism of selective and complete oxidation in La_2O_3-catalyzed oxidative coupling of methane reaction, *Catal. Sci. Technol.*, 2020, **10**, 2602–2614.

35 H. Gao, Y. Xiong, X. Liu, D. Zhao, Y. Feng, L. Wang and J. Wang, A first-principles study of oxygen adsorption on Ir(111) surface, *Appl. Surf. Sci.*, 2016, **389**, 211–215.

36 J. Liu, F. Zhou, Q. Dai and H. Gao, Effect of Ca^{2+}, Mg^{2+}, Ba^{2+} and Sr^{2+} cations on calcium carbonate scaling formation in oil-gas well: based on density functional theory study and molecular dynamics simulation, *J. Cryst. Growth*, 2021, **563**, 126089.

37 M. Irfan, S. Azam and A. Iqbal, Proposal of new stable ABC_2 type ternary semiconductor pnictides $K_3Cu_3P_2$ and $K_3Ni_3P_2$: first-principles calculations and prospects for thermosphysical and optoelectronic applications, *Int. J. Energy Res.*, 2020, **45**, 2980–2996.

38 A. Nadeem, A. I. Bashir, S. Azam, A. U. Rahman and M. A. Iqbal, First-principles quantum analysis on the role of V-doping on the tuning of electronic and optical properties of spinel oxides $MnTi_2O_4$, *Mater. Sci. Eng., B*, 2022, **278**, 115643.

39 S. Alnujaim, A. Bouhemadou, A. Bedjaoui, S. Bin-Omran, Y. Al-Douri, R. Khenata and S. Maabed, *Ab initio* prediction of the elastic, electronic and optical properties of a new family of diamond-like semiconductors, Li_2HgMS_4(M = Si, Ge and Sn), *J. Alloys Compd.*, 2020, **843**, 155991.

40 Y. Zhang and Q. Hou, First-principle study on the effect of point defects on the mechanical properties, thermal conductivity, and optical properties of wurtzite AlN, *Vacuum*, 2023, **207**, 111694.

41 T. Hieu and T. Nguyen, Energy-loss function including damping and prediction of plasmon lifetime, *J. Electron Spectrosc. Relat. Phenom.*, 2014, **193**, 79–85.